Applied Catalysis B: Environmental 176–177 (2015) 570–577

Contents lists available at ScienceDirect

Applied Catalysis B: Environmental

journal homepage: www.elsevier.com/locate/apcatb

Catalytic role and location of Cs promoter in Cs–Au/TiO_2 catalysts for propanol synthesis from CO_2, C_2H_4 and H_2

Stefan J. Ahlers, Marga-Martina Pohl, Joerg Radnik, David Linke, Evgenii V. Kondratenko*

Leibniz-Institut für Katalyse e.V. an der Universität Rostock, Albert-Einstein-Str. 29 A, 18059 Rostock, Germany

ARTICLE INFO

Article history:
Received 31 January 2015
Received in revised form 9 April 2015
Accepted 16 April 2015
Available online 17 April 2015

Keywords:
CO_2 conversion
Propanol
Au nanoparticles
Hydroformylation

ABSTRACT

A series of Cs–Au/TiO_2 (anatase) catalysts with a Cs loading between 0 wt% and 13 wt% was synthesized by impregnation of Au/TiO_2 and tested for CO_2 conversion with C_2H_4 into propanol in presence of H_2. Cs loading was found to significantly influence the target selectivity, which passes over a maximum over the catalysts with 4 wt% and 7 wt% Cs. The results of catalysts characterization by various spectroscopic techniques (HAADF-STEM, XPS, and UV–vis) revealed that Cs species are located on both the support and the Au NP and favor stabilization of $Au^{\delta+}$ species. The presence of Cs was also established to increase the rate of CO insertion into C_2H_4; thus, improving the selectivity to propanol. The positive effect disappears for the catalysts with Cs loading above 7 wt%, which possess larger Au NP (around 17 nm) than the selective catalysts (1–7 wt% Cs) with Au NP between 4.5 nm and 7 nm.

1. Introduction

Under consideration of limited resources of fossil carbon-containing feedstock and current environmental legislation, the modern chemical industry is seeking for alternative syntheses routes and carbon sources to produce fuels and commodity chemicals. Since the last 10 years, plant-derived materials (biomass) and CO_2 have attracted the attention of both academia and industry. Recent developments in biomass conversion into useful products are thoroughly described in [1–4], while CO_2-based approaches are reviewed in [5–7]. Using CO_2 would also diminish its concentration in the atmosphere and thus could contribute to reducing emissions of green-house gases and controlling the global warming [8]. This is particularly valid when CO_2 is converted into long-time stable and usable products like polymers, dyes, or resins. These products are currently produced on the basis of ethylene and/or propylene originating from fossil carbon-containing feedstock. These olefins can be alternatively produced from CO_2 in two steps: (i) methanol synthesis [7–11] and (ii) methanol conversion to olefins (MTO) [12,13]. However, the MTO process suffers from high temperatures and catalyst deactivation caused by coke deposition. To restore initial performance, all known MTO catalysts must be oxidatively regenerated thus resulting in CO_2 formation. Recently, we demonstrated a direct conversion of CO_2 with H_2 and C_2H_4 into 1-propanol (propanol) over TiO_2-supported Au-containing catalysts [14]. No catalyst deactivation was observed over 250 h on stream. This alcohol can be easily dehydrated to propylene [15]. From a mechanistic viewpoint, propanol formation is initiated by CO_2 conversion into CO via the reverse water-gas shift reaction (RWGS) [16,17]. In a second step, the in-situ produced CO is inserted into C_2H_4 (hydroformylation) yielding propanal [18], which is further hydrogenated to propanol. This novel approach is sustainable because C_2H_4 can be derived from biomass (e.g., bio-ethanol) [19], while H_2 can be produced through water splitting.

Despite the near-to 100% propanol selectivity with respect to CO_2, an overall performance of K-Au/TiO_2 materials is low because ethylene is strongly hydrogenated to ethane [14]. This non-desired reaction can be partially suppressed when using catalyst with K loading above 2 wt%. However, the high concentration of the promoter negatively influenced the CO_2 conversion due to the formation of ionic carbonates, which are stable against decomposition to CO required for the hydroformylation step. This drawback may be overcome when using Cs instead of K for promoting Au/TiO_2 because less stable carbonates are formed over Cs_2O [20,21]. Furthermore, Cs should be visible in HAADF-STEM (high-angle annular dark field scanning transmission electron microscopy) analysis owing to its high atomic weight [22,23]. Thus, this technique could help to identify the location of Cs on the surface of catalysts that was not possible in case of K. Such important information may be useful for further catalyst design. Campos-Martín et al. [24] proposed that Cs as a promoter for Cu–Zn–Cr oxide catalysts is highly dispersed over the surface. Larichev et al. [25] reported that Cs in

* Corresponding author. Tel.: +49 3811281290; fax: +49 381128151290.
E-mail address: evgenii.kondratenko@catalysis.de (E.V. Kondratenko).

http://dx.doi.org/10.1016/j.apcatb.2015.04.034
0926-3373/

promoted Ru/C catalysts is located on the active metal and on the support.

The purpose of this work was to investigate whether and how promoting of Au/TiO_2 (anatase) with Cs_2O influences propanol synthesis from CO_2 in the presence of C_2H_4 and H_2. The focus was set on the identification of the promoter location and on the elucidation of its influence on the electronic and catalytic properties of Au nanoparticles. To this end, we prepared $Cs–Au/TiO_2$ catalysts with a fixed Au loading of 2 wt% but different Cs loading (0–13 wt%) and characterized them by HAADF-STEM and ABF-STEM (annular bright field scanning transmission electron microscopy), XPS (X-ray photoelectron spectroscopy) and in situ UV–vis (Ultraviolet–visible) spectroscopy. CO_2 conversion into propanol was studied at 2 MPa under continuous-flow conditions at 473 K and 523 K. In order to identify common factors influencing selectivity and activity, the results of catalytic tests will be related to physico-chemical properties of $Cs–Au/TiO_2$.

2. Experimental

2.1. Preparation of catalysts

Au/TiO_2 (anatase) was prepared by deposition–precipitation of gold hydroxide from $HAuCl_4$ (41.1 wt% Au, Chempur) on the support as follows. 2 g of TiO_2 powder were added at room temperature under continuous stirring to a 1.57 mM $HAuCl_4$ solution (200 ml) and further stirred for 20 min. Afterwards, a NH_3 solution (25%, Roth) was slowly added until pH 10.5 was reached. After 10 min aging phase, the solid was filtered, washed, and finally dried in air at 353 K to yield Au/TiO_2. $Cs–Au/TiO_2$ catalysts were similarly prepared like Au/TiO_2. Here, deposition was done with 0.5 ml NH_3 (25%, Roth) solution. Next step was the incipient wetness impregnation of dried Au/TiO_2 with a $CsNO_3$ solution (99.9%, Chempur). The Cs loading was varied from 1 wt% to 13 wt% Cs. The catalysts were denoted xCs–Au/TiO_2, where "x" stands for the particular Cs weight concentration (Table 1). All catalysts were calcined in air at 573 K for 4 h and finally pressed and sieved to yield a fraction of 250–450 μm.

2.2. Characterization of catalysts

The weight concentration of Au in calcined catalysts was determined by inductively coupled plasma optical emission spectrometry (ICP-OES) using a Varian 715 emission spectrometer.

Nitrogen adsorption–desorption isotherms for all catalysts were collected at 77 K on a BELSORP-mini II (BEL Japan, Inc.) setup. The specific surface area was calculated from the adsorption applying the Brunauer–Emmett–Teller equation for the N_2 relative pressure range of $0.05 < P/P^0 < 0.30$.

The TEM measurements were performed at 200 kV with an aberration-corrected JEM-ARM200F (JEOL, Corrector: CEOS). The microscope is equipped with a JED-2300 (JEOL) energy-dispersive X-ray-spectrometer (EDXS) for chemical analysis. The HAADF-STEM and ABF-STEM measurements were performed with a spot size of approximately 0.13 nm, a convergence angle of 30–36° and collection semi-angles of 90–170 mrad and 11–22 mrad, respectively. The sample was deposed without any pretreatment on a holey carbon supported Cu-grid (mesh 300) and transferred to the microscope. To estimate size distribution of supported Au nanoparticles (NP), at least 100 particles were counted with ImageJ [26].

XP spectra were recorded using a VG ESCALAB 220iXL instrument with monochromatic Al Kα radiation (E = 1486.6 eV). Peaks were fitted to Gaussian–Lorentzian curves after Shirley background subtraction. The electron binding energy was referenced to the Ti $2p_{3/2}$ peak of TiO_2 at 458.8 eV. For quantitative analysis, the peak areas were determined and divided by the element-specific Scofield factor and the detector-depending transmission function.

In situ UV–vis analysis was performed in a setup explained elsewhere [27]. Shortly, ABF-STEM spectra were collected using an AvaSpec UV–vis is spectrometer (Avantes) equipped with a DH-2000 deuterium-halogen light source and a CCD array detector. $BaSO_4$ was used as a white reference material. High temperature reflection UV–vis probes consisting of six radiating optical fibers and one reading fiber were placed inside the furnace facing the quartz reactors. All spectra were calculated as Kubelka–Munk function $F(R)$ according to Eq. (1):

$$F(R) = \frac{(1 - R_\infty)^2}{2 \times R_\infty} \quad (1)$$

where R_∞ is the reflectance.

2.3. Catalytic testing

Catalytic tests were performed at 473 K and 523 K and 2 MPa using an in-house developed setup equipped with 50 continuous-flow fixed-bed reactors operating in parallel. CO_2 (4.5, Air Liquide), H_2 (5.0, Air Liquide), C_2H_4 (3.0, Linde), and N_2 (5.0, Air Liquide) were the feed components. 300 mg of catalyst (fraction of 250–450 μm) were placed in stainless-steel tube reactors (i.d. 4 mm) with threefold amount of SiC for dilution and heated up to 523 K in a N_2 flow (6.67 ml min^{-1} per reactor). Hereafter, the N_2 flow was replaced by a flow (6.67 ml min^{-1} per reactor) of $CO_2/H_2/C_2H_4/N_2$ = 4:2:1:1 reaction feed for 24 h. This activation procedure was necessary to remove residual nitrates stabilized on the surface of Cs-doped catalysts. Such nitrates were not completely decomposed during catalyst calcination because the temperature was kept low to prevent sintering of Au NP. Then, $CO_2/H_2/C_2H_4/N_2$ feeds (1:1:1:1 and 1:2:1:4) were sequentially fed to the reactors at 473 K and 523 K. In order to derive insights into the effect of CO_2 conversion on products selectivity, the modified contact time was varied from 5 g min l^{-1} to 45 g min l^{-1} using a $CO_2/H_2/C_2H_4/N_2$ = 1:1:1:1 feed. Steady-state data were collected after at least 10 h stabilization under each condition. The reaction products and feed components were analyzed by an on-line GC (Varian CP-3800)

Table 1
Catalysts and their selected physico-chemical and catalytic properties.

Catalyst	Au loading (/wt%)	Nominal Cs loading (/wt%)	$d_{Au\,NP}$ (/nm) [a]	S_{BET} (/$m^2 g^{-1}$) [b]	S_{BET} (/$m^2 g^{-1}$) [c]	$X(C_2H_4)$ (/%) [d]	$X(C_2H_4)$(/%) [e]
TiO_2	–	–	–	58	–		
Au/TiO_2	1.3	–	7.5	52	–	44.1	62.5
$1Cs–Au/TiO_2$	1.7	1	4.5	54	38	66.7	77.4
$2Cs–Au/TiO_2$	1.7	2	6.5	55	48	46.0	65.7
$4Cs–Au/TiO_2$	1.6	4	6.0	51	46	62.4	51.9
$7Cs–Au/TiO_2$	1.8	7	5.0	43	44	13.2	15.9
$10Cs–Au/TiO_2$	1.7	10	17.0	39	38	5.5	9.1
$13Cs–Au/TiO_2$	1.7	13	16.5	33	34	1.7	2.8

[a] $d_{Au\,NP}$ was determined from ABF-STEM of used catalysts; [b] and [c] distinguish between fresh catalysts and those used for 160 h on reaction stream, respectively; [d] at 473 K; [e] at 523 K. General reaction conditions: 2 MPa, contact time of 45 g min l^{-1}, $CO_2/H_2/C_2H_4/N_2$ = 1:1:1:1.

equipped with both flame ionization and thermal conductivity detectors with HP-Plot Q and HP-Plot Q and Molsieve 5A columns, respectively. The yields to propanol, propanal, and CO were calculated on CO_2 basis using Eq. (2) taking into account that one C_3-hydrocarbon/oxygenate molecule is formed from one CO_2 and one C_2H_4. In order to ensure high precision in determining low degrees of CO_2 and C_2H_4 conversion, it was calculated from the yields of reaction products formed from these feed components (Eq. (3)). Each reported data point represents an average value of 3 data points, which were collected on a time scale of at least 15 h. A standard deviation was not worse than 3%. Selectivity was calculated according to Eq. (4).

$$Y_i = \frac{\dot{n}_i}{\dot{n}_{f,0}} \times 100\% \quad (2)$$

$$X_f = \sum_i Y_i \quad (3)$$

$$S_i = \frac{Y_i}{X_f} \times 100\% \quad (4)$$

where $\dot{n}_f$ and $\dot{n}_i$ stand for mole flows of feed components and reaction products, respectively. Subscript 0 is used for inlet mole flows.

3. Results

3.1. Bulk and surface characteristics of Cs–Au/TiO_2

The Au loading measured with ICP-OES and the nominal loading of Cs are given in Table 1. This table also lists the specific surface areas (S_{BET}) of fresh and spent catalysts. There was only a slight decrease in S_{BET} of the supports after Au and Cs deposition up to 4 wt% Cs. The increase became more pronounced when the amount of Cs increased further. The surface area of all catalysts additionally decreased after catalytic tests. This is probably caused by a reaction-induced modification of support surface morphology.

To determine the size of Au nanoparticles (NP) and to derive insights into the location of Cs in Cs–Au/TiO_2 catalysts, we performed HAADF-STEM and ABF-STEM studies. It is worth mentioning that the measurements were carried out with used catalysts, i.e., after catalytic tests. However, to check if the size of the Au NP changed during these tests, fresh 1Cs–Au/TiO_2 was also characterized. Au NP of 5 nm in diameter were identified on the surface of the fresh catalyst, while the used sample possessed 4.5 nm Au NP (Fig. S1 in Electronic supporting information (ESI)).This indicates that the Au NP did not sinter during the catalytic test over 160 h on stream. Table 1 shows an average size of Au NP in all used catalysts. Selected ABF-STEM images and the size distribution diagrams are shown in Figs. S2 and S3 in the ESI. Au/TiO_2 possessed Au NP of 7.5 nm [14]. For the catalysts with Cs loading up to 7 wt%, slightly smaller Au NP in the range between 4.5 nm and 6.5 nm were observed. However, upon further increase in Cs loading, NP became larger, i.e., 17 nm and 16.5 nm for 10Cs–Au/TiO_2 and 13Cs–Au/TiO_2, respectively. At these high dopant concentrations, Cs should already cover the support surface with a monolayer and thus forcing the smaller Au NP to collapse to larger ones.

HAADF-STEM analysis additionally provided an insight into the location of the promoter. High resolution images of selected Cs–Au/TiO_2 catalysts are shown in Fig. 1. Further examples are shown in Fig. S4 in ESI. In addition to the larger white spots representing Au NP, the surface of TiO_2 was populated by small single white spots, which can be ascribed to single atoms of Au or/and Cs. Importantly, EDX analysis on samples with high promoter content revealed that Cs should be present in these spots. Therefore, we assume that Cs is atomically distributed over the surface of catalysts. This assumption is supported by the fact that

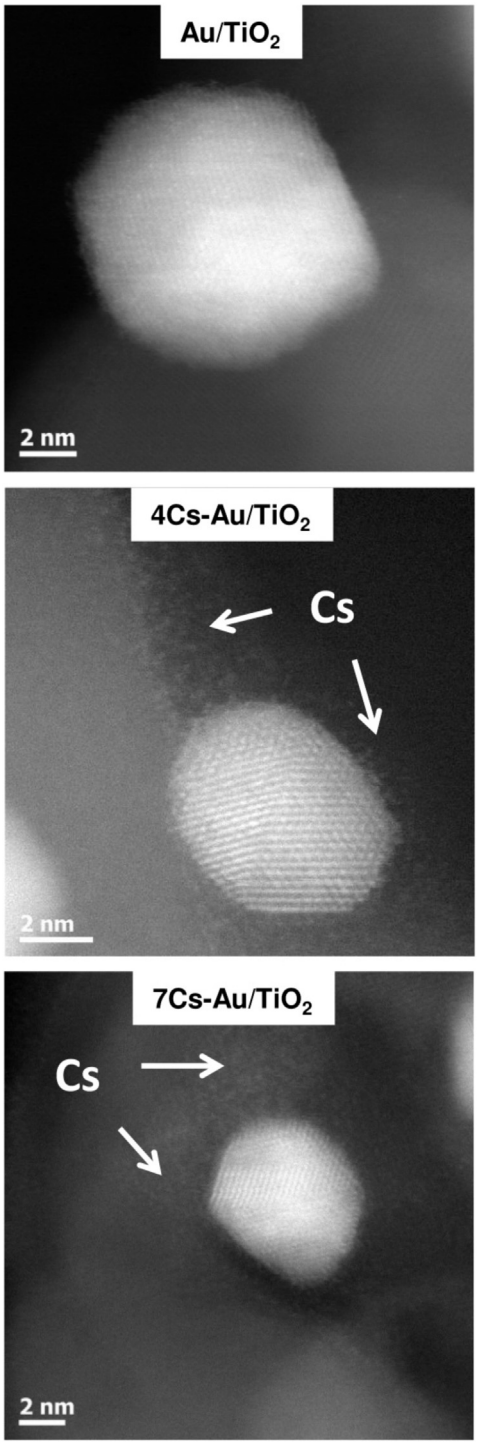

Fig. 1. High resolution HAADF-STEM images of Au/TiO_2, 4Cs–Au/TiO_2, and 7Cs–Au/TiO_2.

the number of small white spots in HAADF-STEM images strongly increased with an increase in Cs loading, while the loading of Au was fixed. Especially, the perimeter of the support, where an apparent agglomeration of single atoms occurred, was suited for a quantitative observation. This is due to the fact that a surface plain covered by Cs was in plain with the laser beam and thus bearing this apparent agglomeration. It is important to highlight that the single Cs atoms did not move during longer exposure time to the laser beam. From a theoretical calculation with the ionic radius and a quadratic orientation of the Cs atoms, a monolayer of Cs should be achieved

from a Cs loading higher than 11.5 wt%. Therefore, the samples with a high amount of Cs (7–13 wt%) showed a good visibility of Cs atoms, which amount increased rapidly and ended up at a visible monolayer in 13Cs–Au/TiO_2.

Upon closer inspection of Au NP, one can see that the Au NP on catalysts with high Cs loading (Fig. 1b) consisted of frayed edges, i.e., there were single atoms located on the surface of Au NP but not belonging to their bulk. Unfortunately, it was experimentally impossible to assign these atoms to Au or Cs with EDX. Therefore, we applied UV–vis and XP spectroscopy to further support our assumption about the presence of Cs on/into Au NP. The results are presented and discussed in the following sections.

3.2. Analysis of oxidation states of Au and Cs

To check the effect of reaction conditions on the oxidation state of Ti, Cs and Au, we analyzed both fresh and used 1Cs–Au/TiO_2, 4Cs–Au/TiO_2, and 13Cs–Au/TiO_2 samples. As expected, Cs was in its highest oxidation state (Cs^+). Only for the fresh catalyst with 13 wt% Cs, two different Cs^+ signals were identified in the XP spectrum (Fig. S5 in ESI). Since the spectrum of the used catalyst is characterized by only one Cs^+ state, we put forward that two states in the fresh samples were Cs_2O and residual $CsNO_3$ with the latter having been reduced under reaction conditions. Titanium was also stabilized in its highest oxidation state (Fig. S6 in ESI).

Fig. 2 shows the Au (Au4f peak) XP spectra of 1Cs–Au/TiO_2, 4Cs–Au/TiO_2, and 13Cs–Au/TiO_2 before and after catalytic tests. The signals were cut off at lower eV due to the upcoming Cs 4d peak, which even influenced the Au signal in the spectrum of the fresh 13Cs–Au/TiO_2 catalyst. For all catalysts, the Au signal can be subdivided into two subsignals indicating two different Au states. The main 4f7/2 peak is at around 83.0 eV, while a less intensive shoulder has higher energy. The Au main peak (metallic Au) is influenced by the TiO_2 support leading to lower binding energies than for bulk metallic Au. Since the electron binding energy of the shoulder peak is higher than that of the main peak, it should correspond to an oxidized Au state. We call this state $Au^{\delta+}$ in order to distinguish it from the metallic Au state (the main peak in Fig. 2). Based on the electron binding energy value, we assume that the signal for the charged Au species does not correspond to Au^{1+} or Au^{3+}. The fraction of each Au signal depended on Cs content and catalyst treatment under $CO_2/H_2/C_2H_4$ conditions. The fresh 1Cs–Au/TiO_2 catalyst possessed both Au^0 and $Au^{\delta+}$ (Fig. 2a), while only Au^0 was identified in the used material. The amount of Au^0 also increased with a simultaneous decrease in the concentration of $Au^{\delta+}$ in 4Cs–Au/TiO_2 after performing catalytic tests (Fig. 2b). However, $Au^{\delta+}$ did not completely disappear as in case of 1Cs–Au/TiO_2. The XP spectrum of fresh 13Cs–Au/TiO_2 is characterized by a broad noisy signal (Fig. 2c), which cannot be interpreted correctly. However, Au^0 and $Au^{\delta+}$ were identified in the XP spectrum of used 13Cs–Au/TiO_2. Comparing the ratio of $Au^{\delta+}/Au^0$ in the used materials, it is obvious that this ratio increased with an increase in Cs loading; used 1Cs–Au/TiO_2 did not even possess $Au^{\delta+}$. The effect of Cs loading on this ratio suggests that Cs favors the stabilization of $Au^{\delta+}$ in Cs–Au/TiO_2. We put forward that $Au^{\delta+}$ can only be formed when Cs atoms are located either on the top of Au NP or even incorporated into these species. We can exclude that $Au^{\delta+}$ can originate on the interface between Au NP and TiO_2 since used 1Cs–Au/TiO_2 did not possess $Au^{\delta+}$. For this catalyst, Cs was either not on the Au NP or its amount was too low to stabilize $Au^{\delta+}$. Increasing the Cs content led to the formation of decent amounts of Cs_2O on/in the Au NP making the stabilization of $Au^{\delta+}$ possible. An inhibiting effect of Cs on the reduction of copper was previously reported for Cs promoted Cu–Zn–Cr oxide catalysts [24].

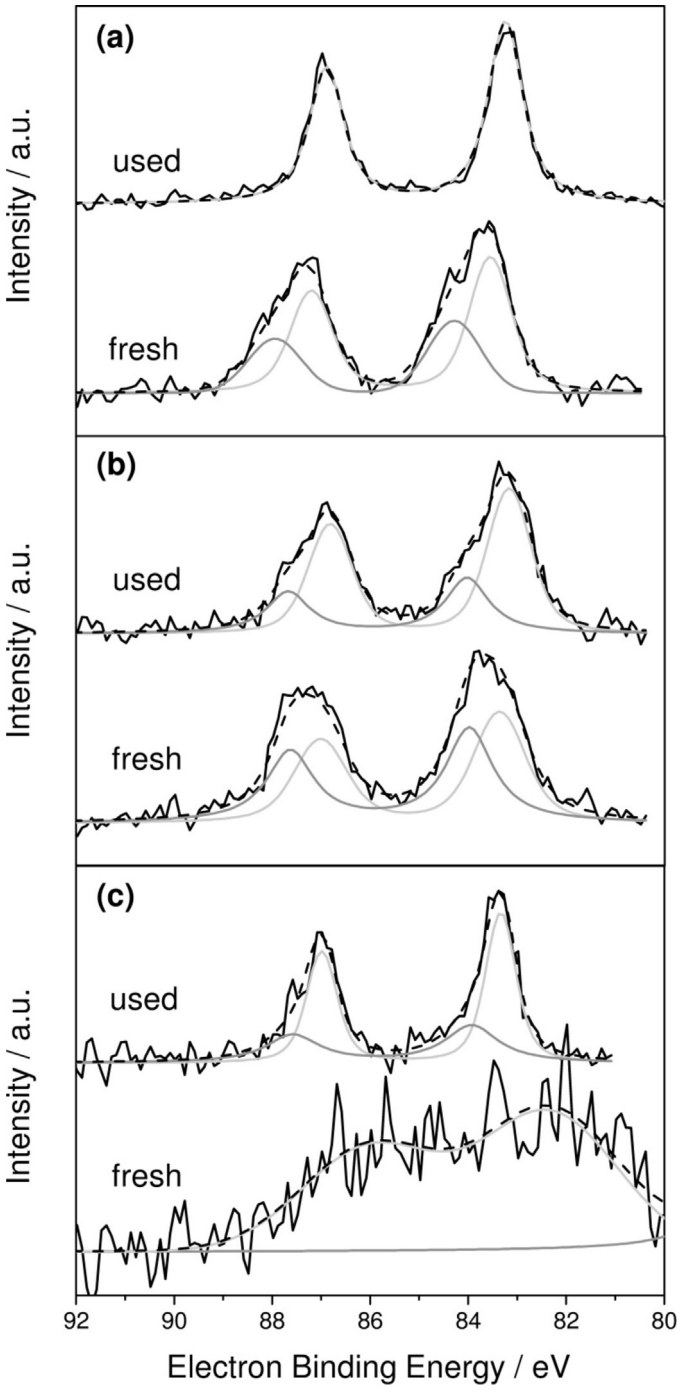

Fig. 2. Au4f XP spectra of fresh and used (a) 1Cs–Au/TiO_2, (b) 4Cs–Au/TiO_2, and (c) 13Cs–Au/TiO_2. The dashed line is fitted to the original signal while the light grey and grey ones correspond to Au^0 and $Au^{\delta+}$, respectively. The signal of fresh 13Cs–Au/TiO_2 is influenced by the Cs 4d signal which could be separated for all other samples.

3.3. Oxidation and reduction behavior of Au NP

To check whether Cs is really located in the vicinity (probably on the top) of Au NP, we performed in situ UV–vis experiments during oxidation and reduction of two representative Au/TiO_2 and 4Cs–Au/TiO_2 catalysts, i.e., without and with Cs. The catalysts were initially heated to 523 K in a flow of nitrogen after an oxidative treatment at same temperature in an air flow. Their UV–vis spectra under nitrogen are shown in Fig. 3. The adsorption with a maximum at ca. 300 nm derived mainly from the band gap transition of TiO_2 [28], while supported Au NP are characterized by

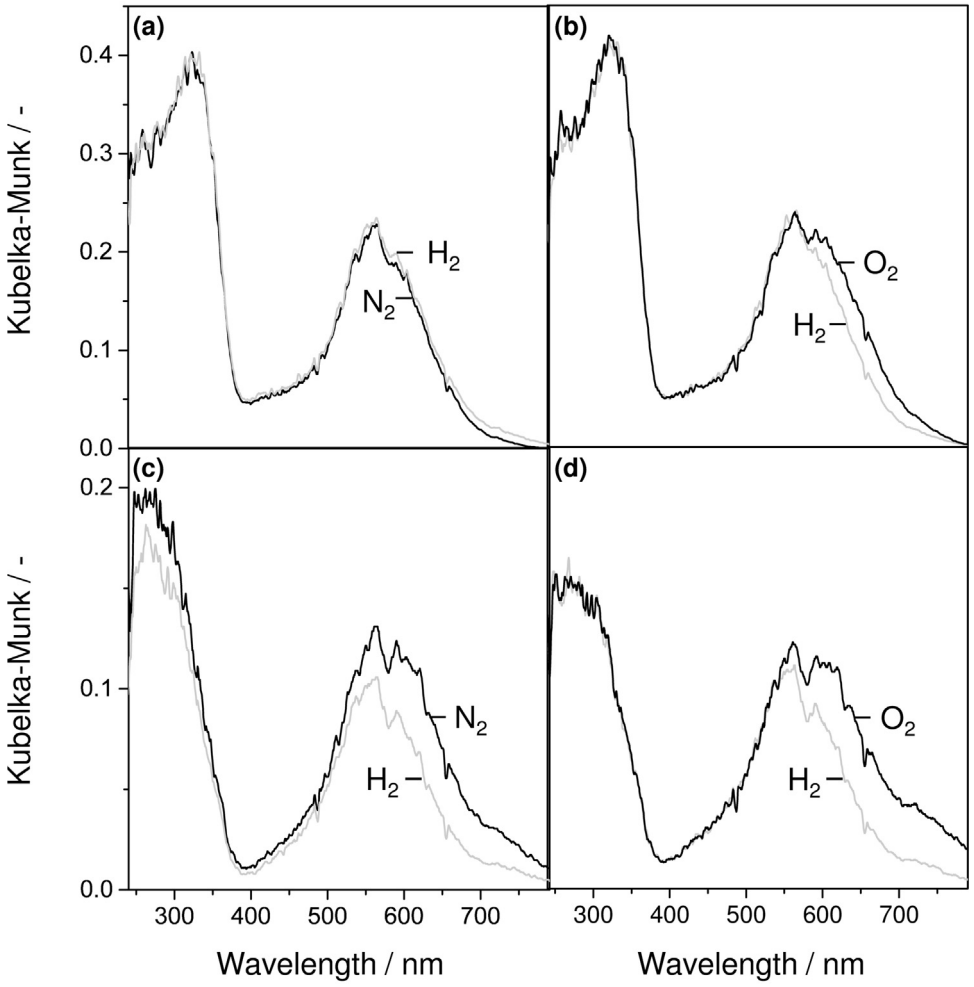

Fig. 3. UV–vis spectra of (a, b) Au/TiO_2 and (c, d) $4Cs–Au/TiO_2$ during the reduction (a, c) and oxidation (b, d) at 523 K and atmospheric pressure within 3 min. The samples were oxidized before the first reduction.

typical surface plasmon resonance (SPR) bands between 400 nm and 800 nm with a maximum at approximately 550 nm [29]. The spectrum of Au/TiO_2 did not change when the catalyst was treated in a H_2-containing flow (20% H_2 in N_2) thus proving that the oxidation state of Ti and Au were same under oxidizing and reducing conditions, i.e., Ti^{4+} and Au^0. However, the intensity of SPR bands in the spectrum of $4Cs–Au/TiO_2$ significantly decreased after the reductive treatment. Since neither the position of UV–vis fiber nor reactor temperature were changed upon switching from N_2 to H_2, such variation in the spectrum should be due to the effect of reaction conditions on the state of Au. For clarifying this effect, we treated the reduced Au/TiO_2 and $4Cs–Au/TiO_2$ catalysts in an air flow at the same temperature. As shown in Fig. 3, the intensity of SPR bands in the spectra of Au/TiO_2 and $4Cs–Au/TiO_2$ increased after such treatment. Such changes in the spectra indicate changes in the size of Au NP. According to [29], the size can be estimated from the ratio of the absorbance at the maximum of SPR (A_{spr}) and a second other absorbance outside the SPR absorbance (e.g., at 450 nm (A_{450})) using Eq. (5). Since, we used the same spectrometer and the catalysts were characterized under same conditions this equation can be simplified to Eq. (6).

$$d_{Au\ NP} = \exp(B_1 \times \frac{A_{SPR}}{A_{450}} - B_2) \quad (5)$$

with B_1 and B_2 being constants of a calibration.

$$d_{Au\ NP} \sim \exp(\frac{A_{SPR}}{A_{450}}) \quad (6)$$

The oxidized catalysts had higher ratio of A_{spr}/A_{450} than their reduced counterparts. This suggests an increase in the size of Au NP after the oxidative treatment. The decrease in the size of AuNP during reduction was in good agreement with the STEM results for fresh and used $1Cs–Au/TiO_2$ catalysts (Fig. S1). Taking into account the results of XPS and STEM analysis, growing and shrinking of Au NP under, respectively, oxidative and reductive conditions can be explained as follows. Upon oxygen treatment, metallic Au^0 species were partially oxidized to $Au^{\delta+}$. To stabilize the charge, some oxygen species should be dissolved into Au NP resulting in an increase in their size. During reduction, these species were removed and thus the NP shrank. Since the above changes in the UV–vis spectra were stronger for $4Cs–Au/TiO_2$ than Au/TiO_2, it can be concluded that formation of $Au^{\delta+}$ is favored in presence of Cs. Under consideration of STEM results, we suggest that Cs_2O is located onto or in the Au NP.

3.4. Activity and selectivity of Cs–Au/TiO$_2$

Differently loaded $Cs–Au/TiO_2$ catalysts were tested for their activity and selectivity in CO_2 conversion to propanol in the presence of C_2H_4 and H_2 at 2 MPa and 473 K and 523 K. We start with the effect of Cs on CO_2 and C_2H_4 conversion. All catalysts are compared

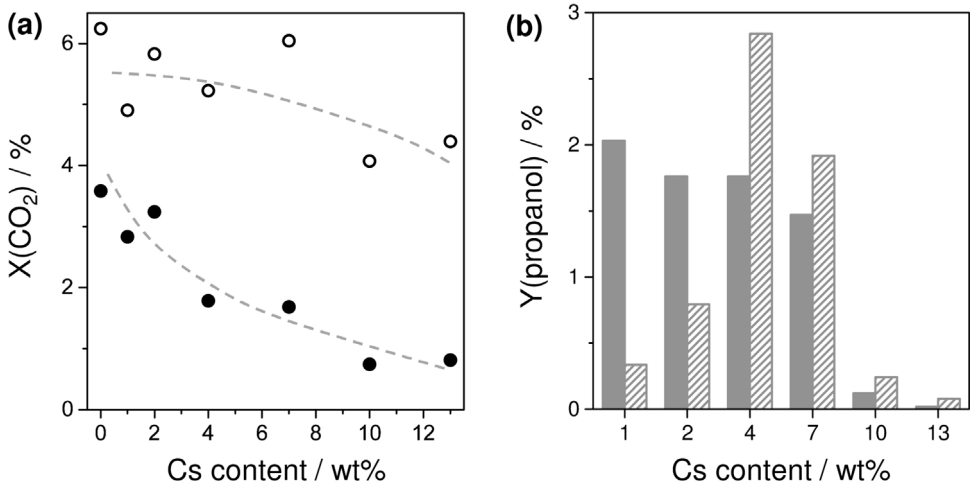

Fig. 4. (a) Conversion of CO_2 and (b) yield of propanol at 473 K (closed symbols/bars) and 523 K (open symbols, dashed bars) against Cs content on Au/TiO_2. Reaction conditions: 2 MPa, contact time of 45 g min l^{-1}, $CO_2/H_2/C_2H_4/N_2$ = 1:1:1:1.

at same contact time (τ) of 45 g min l^{-1}. Fig. 4(a) shows the conversion of CO_2 as a function of Cs loading. Au/TiO_2 revealed the highest conversion at both temperatures. Promoting with Cs resulted in a decrease in the conversion. At 473 K, it dropped continuously from 3.6% over Au/TiO_2 to only 0.7% over 13Cs–Au/TiO_2. Logically, the conversion over all catalysts increased with an increase in temperature to 523 K. Analogously to 473 K, it decreased with Cs content but the decrease was less pronounced, i.e., from 6.2% over Au/TiO_2 to 4.1% over 10Cs–Au/TiO_2. This indicates that the activation energy of CO_2 conversion increased with Cs loading. This loading also influenced the conversion of C_2H_4 (Table 1). It should be noted that this conversion was significantly higher than the conversion of CO_2 over catalysts with low Cs loading. This is due to the fact that C_2H_4 was not only converted to propanal/propanol but mainly hydrogenated to C_2H_6. Further side reaction was C_2H_4 dimerization to butenes, which were, however, formed in traces and only at 523 K. At both temperatures, C_2H_4 conversion passed over a maximum at a Cs loading of 1 wt% and decreased almost continuously with an increase in the loading to 13 wt% Cs from 67% to 2% and from 77% to 3% at 473 K and 523 K, respectively.

CO, propanal, and propanol were the main reaction products formed from CO_2. Propane and hexanes were formed in traces. In order to exclude the effect of CO_2 conversion on products selectivity, we performed additional catalytic tests to achieve an iso-conversion of CO_2 of around 2% and 5% at 473 K and 523 K, respectively. Fig. 5 illustrates the selectivity to CO, propanal, and propanol calculated on CO_2 basis according to Eq. (4). Propanal as another desired product was usually obtained with a selectivity not higher than 5%. Therefore, the below discussion is related to CO and propanol. As in case of C_2H_4 conversion, the selectivity to propanol passed a maximum with rising Cs loading from 0 to 13 wt%. However, the highest propanol selectivity of 99% and 54% was determined over 4Cs–Au/TiO_2 at 473 K and at 523 K, respectively. A combined oxo-selectivity (propanol + propanal) of 100% was achieved over this catalyst at 473 K. Au/TiO_2 did not produce propanol at 523 K, while the corresponding selectivity at 473 K was only around 18%. Such low or even worse performance was obtained over catalysts with 10 wt% and 13 wt% Cs as well. All other catalysts performed superior to these three materials but were less selective than 4Cs–Au/TiO_2.

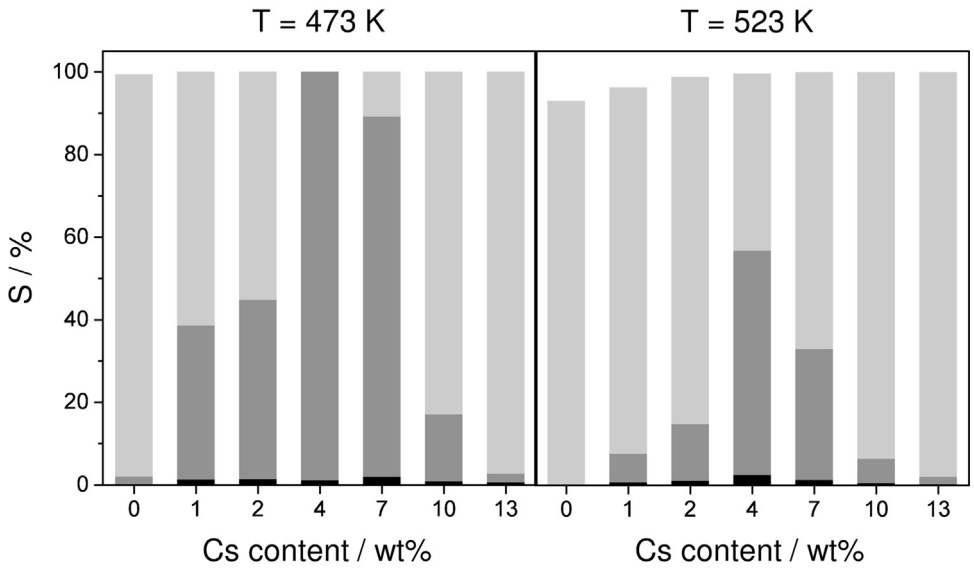

Fig. 5. Selectivity to CO (light grey bar), propanol (grey bar), and propanal (black bar) based on CO_2 against Cs content on Cs–Au/TiO_2 at 473 K and 523 K and CO_2 conversion of 2% and 5%, respectively.

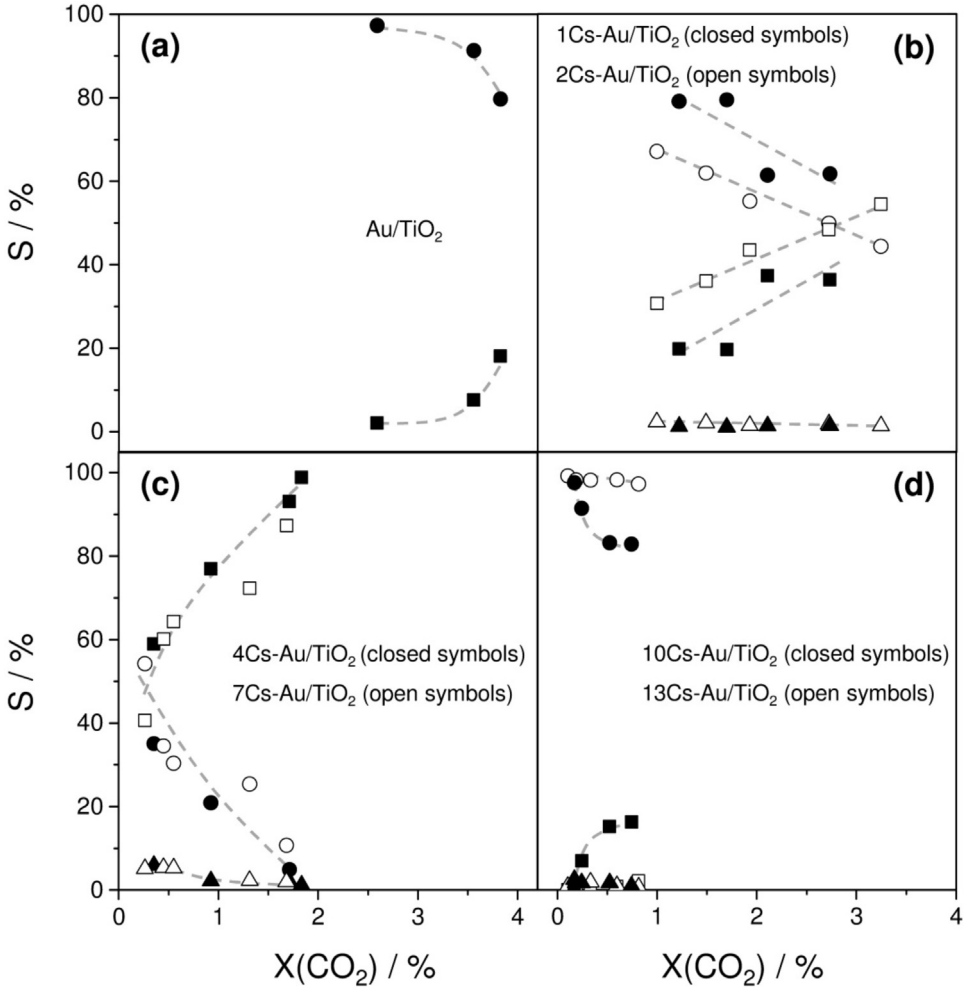

Fig. 6. Effect of CO_2 conversion on the selectivity to CO (● and ○), propanal (▲ and △), and propanol (■ and □) over (a) Au/TiO_2, (b) 1Cs–Au/TiO_2 and 2Cs–Au/TiO_2, (c) 4Cs–Au/TiO_2 and 7Cs–Au/TiO_2, and (d) 10Cs–Au/TiO_2 and 13Cs–Au/TiO_2 at 2 MPa and 473 K using a $CO_2/H_2/C_2H_4$ = 1:1:1 feed.

For deriving insights into overall reaction pathways leading from CO_2 to propanol, we performed catalytic tests at different contact times to achieve different degrees of CO_2 conversion; the longer the contact time, the higher the conversion is. Fig. 6 shows the selectivity-conversion plots for all Cs–Au/TiO_2 catalysts. In general, CO selectivity decreases with rising CO_2 conversion, while propanol selectivity increases. The selectivity to propanal is always below 5% and decreases with CO_2 conversion. Similar selectivity-conversion profiles were previously reported by us for K-Au/TiO_2 catalysts [14]. From a mechanistic viewpoint, such effect of CO_2 conversion on products selectivity can be explained as follows. CO_2 is primarily converted to CO through the RWGS reaction. Such in situ formed CO is inserted into C_2H_4 to yield propanal, which is further hydrogenated to propanol. Since the overall reaction scheme is valid for all catalysts irrespective of Cs loading, we put forward that the loading influences the kinetics of individual reaction pathways and thus determines the distinct catalyst selectivity in Fig. 5. The below discussion is aimed at elucidating possible origins of the promoter effect on catalytic performance.

4. Discussion

Fig. 6 clearly shows that no propanol was observed over Au/TiO_2 at a CO_2 conversion below 2%. In contrast, catalysts with a Cs loading between 1 wt% and 7 wt% produced propanol even at the conversion below 1%. Traces of propanol were also observed over 10Au–Cs/TiO_2 and 13Cs–Au/TiO_2, which showed the less marked decrease in CO selectivity with increasing degree of CO_2 conversion. The strongest effect of the conversion on the selectivity to CO and propanol was achieved over the catalysts with 4 wt% and 7 wt% Cs. Moreover, they were able to generate propanol with the selectivity above 50% even at a CO_2 conversion of only 0.3%. Changes in the selectivity to CO and propanol with an increase in CO_2 conversion became less pronounced with a decrease or increase in Cs content.

Taking into account the overall scheme of CO_2 transformation into propanol, the effect of Cs loading on the selectivity-conversion profiles in Fig. 6 can only be explained by the interplay between the kinetics of (i) CO formation from CO_2 and (ii) CO insertion into C_2H_4 to yield propanal, which is fast hydrogenated to propanol. For Au/TiO_2, 10Cs–Au/TiO_2, and 13Cs–Au/TiO_2, the weakest obtained effect of CO_2 conversion on CO selectivity suggests that the rate of CO generation was significantly higher than the rate of CO reaction with C_2H_4 to yield propanal. The difference between these rates became smaller when Cs loading increased from 0 wt% to 1 wt% and 2 wt% and reached the lowest value for the catalysts with 4 wt% and 7 wt% Cs.

Bearing in mind mechanistic similarities of CO_2 conversion into propanol between Cs–Au/TiO_2 and previously tested K-Au/TiO_2 [14], we put forward that promoting of Au/TiO_2 with Cs also improved activation of H_2 and thus accelerated the hydroformylation of ethylene to propanal. In addition, the present study revealed that Cs located on or inside the Au NP favored the formation of

partially charged $Au^{\delta+}$ species. Actually, such sites played a positive role for the adsorption and activation of CO [30–32]. When correlating the selectivity to propanol with the concentration of $Au^{\delta+}$ determined from XPS, we suggest that positively charged Au species enhanced the selectivity to propanol owing to the improved ability of CO insertion into ethylene to yield propanal. However, the positive effect of doping decreased at Cs loadings above 7 wt% owing to the formation of Cs_2O monolayer and thus covering the active surface of Au NP.

Since both CO generation/activation and C_2H_4 adsorption/activation can influence the rate of propanol formation, we now elaborate on the effect(s) of Cs loading on CO_2 and C_2H_4 conversion. From Fig. 4(a) and Table 1, it is obvious that the conversion of CO_2 at 473 K continuously decreased with Cs loading but was more stable at 523 K. Contrarily, the conversion of ethylene at both temperatures did not show any clear dependence on Cs loading in the range between 0 wt% and 4 wt%, but significantly dropped at higher loadings. These dissimilar dependences of CO_2 and C_2H_4 conversion suggest that CO_2 and C_2H_4 were activated on different sites. CO_2 was adsorbed and reduced to CO on the support at the perimeter of Au NP where adsorbed hydrogen species were present [33]. In contrast, C_2H_4 hydrogenation and hydroformylation occurred on the surface of Au NP [14]. Therefore, the strong decrease in C_2H_4 conversion over catalysts with Cs loading above 4 wt% can be explained by the fact that ethylene adsorption/conversion was strongly inhibited upon approaching Cs_2O monolayer. Cs blocks active sites on Au NP and decreases catalyst acidity thus hindering ethylene adsorption. Importantly, 7Cs–Au/TiO_2 was significantly less active for ethylene conversion than the catalysts with lower Cs loading (Table 1), but produced propanol very selectively (Fig. 5).Contrarily, 10Cs–Au/TiO_2 and 13Cs–Au/TiO_2 also showing low ethylene conversion were not selective. Thus, the Cs loading is not the only factor determining propanol selectivity. The size of Au NP should also play an important role for propanol formation (Fig. 4(b) and Table 1). Based on the results of STEM analysis, we can conclude that Cs–Au/TiO_2 catalysts with Au NP larger than 10 nm are not selective for propanol synthesis. This is in good agreement with the results previously reported for K-Au/TiO_2 [14].

When comparing catalytic performance of K-Au/TiO_2 [14] and Cs–Au/TiO_2 both possessing similarly sized Au NP, Cs appears to be more suitable dopant. Promoting of Au/TiO_2 with Cs enables to operate selectively at 523 K, where higher CO_2 conversion was achieved thus resulting in higher yield of propanol. The highest yield of propanol of 2.9% was achieved in the present study compared to 2.4% previously reported for K-Au/TiO_2. Another advantage of the Cs–Au/TiO_2 system is relatively high selectivity to propanol calculated on C_2H_4 basis. The highest value of 13% was obtained over 7Cs–Au/TiO_2, while the corresponding value for K-Au/TiO_2 catalysts was not higher than 3%. This means that non-desired ethylene hydrogenation to ethane was strongly suppressed over 7Cs–Au/TiO_2.

5. Conclusions

Cs loading and the size of Au NP were demonstrated to have a strong effect on the activity and particularly selectivity of Cs–Au/TiO_2 catalysts in the conversion of CO_2 and C_2H_4 into propanol in presence of H_2. Since the overall scheme of products formation was valid for all catalysts, it was concluded that the key steps of this conversion, i.e., CO generation and insertion into ethylene to form propanal, were controlled by the above catalyst characteristics. As proven by HAADF-STEM and EDX, Cs was homogenously distributed on the support and was also located on/into Au NP. The presence of the alkali ions in the latter case was important (i) to stabilize $Au^{\delta+}$ species required for CO activation and insertion into ethylene resulting in propanal and (ii) to suppress non-selective ethylene hydrogenation to ethane. The latter reaction was also strongly influenced by the size of Au NP. The NP of 17 nm at high Cs loading (>7 wt%) showed significantly lower activity for ethane formation than ones of 4.5–7.5 nm. The derived mechanistic knowledge opens the possibility for the design of highly selective and catalysts for converting CO_2 into propanol via the size of Au NP and nature/concentration/location of promoter.

Acknowledgements

The authors thank gratefully Anja Simmula for the ICP-OES and Carsten Kreyenschulte for additional help for recording STEM images. This work was supported by the Leibniz-Gemeinschaft under the research grant SAW-2011-LIKAT-2.

Appendix A. Supplementary data

Supplementary data associated with this article can be found, in the online version, at http://dx.doi.org/10.1016/j.apcatb.2015.04.034.

References

[1] H. Balat, Energy Educ. Sci. Tech. 24 (2010) 85–111.
[2] E. Taarning, C.M. Osmundsen, X.B. Yang, B. Voss, S.I. Andersen, C.H. Christensen, Energy Environ. Sci. 4 (2011) 793–804.
[3] A. Tanksale, J.N. Beltramini, G.M. Lu, Renew. Sustain. Energy Rev. 14 (2010) 166–182.
[4] P.Y. Dapsens, C. Mondelli, J. Pérez-Ramírez, ACS Catal. 2 (2012) 1487–1499.
[5] W. Wang, S. Wang, X. Ma, J. Gong, Chem. Soc. Rev. 40 (2011) 3703–3727.
[6] G. Centi, E.A. Quadrelli, S. Perathoner, Energy Environ. Sci. 6 (2013) 1711–1731.
[7] E.V. Kondratenko, G. Mul, J. Baltrusaitis, G.O. Larrazábal, J. Pérez-Ramírez, Energy Environ. Sci. 6 (2013) 3112–3135.
[8] M. He, Y. Sun, B. Han, Angew. Chem. Int. Ed. 52 (2013) 9620–9633.
[9] S.G. Jadhav, P.D. Vaidya, B.M. Bhanage, J.B. Joshi, Chem. Eng. Res. Des. 92 (2014) 2557–2567.
[10] G.A. Olah, Angew. Chem. Int. Ed. 52 (2013) 104–107.
[11] G. Centi, S. Perathoner, ChemSusChem 3 (2010) 195–208.
[12] U. Olsbye, S. Svelle, M. Bjørgen, P. Beato, T.V.W. Janssens, F. Joensen, S. Bordiga, K.P. Lillerud, Angew. Chem. Int. Ed. 51 (2012) 5810–5831.
[13] J. Lefevere, S. Mullens, V. Meynen, J. Van Noyen, Chem. Pap. 68 (2014) 1143–1153.
[14] S.J. Ahlers, U. Bentrup, D. Linke, E.V. Kondratenko, ChemSusChem 7 (2014) 2631–2639.
[15] A.J. Papa, Ullmann's Encyclopedia of Industrial Chemistry, Wiley-VCH Verlag GmbH & Co., KGaA, 1993.
[16] H. Sakurai, A. Ueda, T. Kobayashi, M. Haruta, Chem. Commun. (1997) 271–272.
[17] R. Burch, Phys. Chem. Chem. Phys. 8 (2006) 5483–5500.
[18] X. Liu, B. Hu, K. Fujimoto, M. Haruta, M. Tokunaga, Appl. Catal. B 92 (2009) 411–421.
[19] S.P. Pyl, C.M. Schietekat, M.-F. Reyniers, R. Abhari, G.B. Marin, K.M. Van Geem, Chem. Eng. J. 176–177 (2011) 178–187.
[20] A. Zukal, J. Pawlesa, J. Čejka, Adsorption 15 (2009) 264–270.
[21] E.J. Doskocil, G.M. Mueller, J. Catal. 234 (2005) 143–150.
[22] Y.V. Larichev, J. Phys. Chem. C 115 (2010) 631–635.
[23] Y.V. Larichev, B.L. Moroz, E.M. Moroz, V.I. Zaikovskii, S.M. Yunusov, E.S. Kalyuzhnaya, V.B. Shur, V.I. Bukhtiyarov, Kinet. Catal. 46 (2005) 891–899.
[24] J.M. Campos-Martín, J.L.G. Fierro, A. Guerrero-Ruiz, R.G. Herman, K. Klier, J. Catal. 163 (1996) 418–428.
[25] Y.V. Larichev, D.A. Shlyapin, P.G. Tsyrul'nikov, V.I. Bukhtiyarov, Catal. Lett. 120 (2008) 204–209.
[26] T.J. Collins, BioTechniques 43 (2007) S25–S30.
[27] O. Ovsitser, M. Cherian, A. Brückner, E.V. Kondratenko, J. Catal. 265 (2009) 8–18.
[28] T. Kako, N. Umezawa, K. Xie, J. Ye, J. Mater. Sci. 48 (2013) 108–114.
[29] W. Haiss, N.T.K. Thanh, J. Aveyard, D.G. Fernig, Anal. Chem. 79 (2007) 4215–4221.
[30] Q. Fu, H. Saltsburg, M. Flytzani-Stephanopoulos, Science 301 (2003) 935–938.
[31] Q. Fu, W. Deng, H. Saltsburg, M. Flytzani-Stephanopoulos, Appl. Catal. B 56 (2005) 57–68.
[32] P. Kast, G. Kučerová, R.J. Behm, Catal. Today 244 (2015) 146–160.
[33] E. Bus, J.A. van Bokhoven, Phys. Chem. Chem. Phys. 9 (2007) 2894–2902.